Changes in the partial pressure of carbon dioxide in the Mauritanian-Cape Verde upwelling region between 2005 and 2012.

By

Melchor González-Dávila[1*], J. Magdalena Santana Casiano[1] and Francisco Machín[1,2]

[1]Instituto de Oceanografía y Cambio Global, Grupo QUIMA, Universidad de Las Palmas de Gran Canaria, 35017, Las Palmas de Gran Canaria. Spain.

[2]Departamento de Física, Universidad de Las Palmas de Gran Canaria, 35017, Las Palmas de Gran Canaria

***** Correspondence to melchor.gonzalez@ulpgc.es

ABSTRACT

Coastal upwelling along the eastern margins of major ocean basins represent regions of large ecological and economic importance due to the high biological productivity. The role of these regions in the global carbon cycle makes them essential in addressing climate change. The physical forcing of upwelling processes that favor the production in these areas are already being affected by global warming, which will modify the intensity of the upwelling and, consequently, the carbon dioxide cycle. Here, we present monthly high resolution surface experimental data for temperature and partial pressure of carbon dioxide in one of the four most important upwelling regions of the planet, the Mauritanian-Cape Verde upwelling region, from 2005 to 2012. This data set provides direct evidence of seasonal and interannual changes in the physical and biochemical processes. Specifically, we show an upwelling intensification and an increase of 0.6 Tg a year in CO_2 outgassing due to increased wind speed, despite increased primary productivity. This increase in CO_2 outgassing together with the observed decrease in sea surface temperature at the location of the Mauritanian Cape Blanc, 21ºN, produced a pH decrease of -0.003 ± 0.001 per year.

1. INTRODUCTION

The excess of CO_2 in the atmosphere, largely responsible for global climate change, has prompted research on the role of the oceans in the carbon cycle. The aim in recent decades has been to assess how the oceans act as sources or sinks within the carbon cycle. To achieve this goal, hight spatial and temporal observations representative of the distribution of CO_2 fluxes between the ocean and atmosphere are necessary. Automated instruments on volunteer observing ships (VOS) serve to provide as many observations throughtout the global ocean as possible, in addition to the data collected on scientific cruises and at long-term moorings (i.e., Astor et al., 2005: Lüger et al., 2004, 2006; González-Dávila et al., 2005; 2009; Schuster et al., 2009; Ullman et al., 2009; Watson et al., 2009; Padín et al., 2010; Gruber et al., 2002; Dore et al., 2003; Santana-Casiano et al., 2007; Bates et al., 2014).

With the amount of data already gathered (http://www.socat.info/), climatologies that present average fluxes between the atmosphere and the ocean have been developed, identifying areas acting as a source or sink (Key et al., 2004; Takahashi et al., 2009). However, the low spatial resolution of these databases limits the applicability especially in coastal areas. Upwelling regions are particularly under-represented in such large databases. Upwelling presents a dynamic process that raises nutrient and CO_2 rich water from relatively deep areas to the surface. The nutrients reaching the photic zone promote primary production, which consumes CO_2. This process generates a CO_2 flux into the ocean. On the other hand, the upwelling also brings up CO_2 from deep seawater, which generates uncertainty about the actual role of upwelling areas as a source or sink of CO_2 (Michaels et al., 2001). Indeed, upwelling areas may act as a source or sink of CO_2 depending on their location (Cai et al., 2006; Chen et al., 2013), where upwelling regions at low latitudes mainly act as a source of CO_2 (Feely et al., 2002; Astor et al., 2005; Friederich et al., 2008; Santana-Casiano et al., 2009; González-Dávila et al., 2009) and those at mid-latitudes mainly act as a sink of CO_2 (Frankignoulle and Borges, 2001; Hales et al., 2005; Borges et al., 2002; 2005; Santana-Casiano et al., 2009; González-Dávila et al., 2009). Several anthropogenic interactive effects strongly influence Eastern Boundary Upwelling Systems (EBUS), including upper ocean warming, ocean acidification and ocean deoxygenation (Gruber, 2011; Feely et al., 2008; Keeling et al., 2010). Moreover, evidence of increasee wind speed that would favor upwelling (Bakun, 1990; Demarcq, 2009; Oerder et al., 2015) supports the possibility of a change in the dynamics of these highly productive areas. Recently, eddy-resolving regional ocean models have shown how upwelling intensification can cause a major impact on the system's biological productivity and CO_2 outgassing (Lachkar and Gruber, 2013; Oerder et al., 2015). Wind observations and reanalysis products are controversial regarding the Bakun intensification hypothesis (Bakun 1990). Using different wind databases for the Canary region, Barton et al. (2013) concluded that there was no evidence for a general increase in the upwelling intensity off northwest Africa while Marcello et al. (2011) found an intensification of the upwelling system in the same area during a 20-year period while the alongshore wind stress remained almost stable. Cropper et al. (2014) found that coastal summer wind speed increased, resulting in an increase in upwelling-favorable wind speeds north of 20ºN and an increase in downwelling-favorable winds south of 20ºN. Santos et al. (2005; 2012) showed Sea Surface Temperature (SST) was not homogeneous either along latitude or longitude and depending on the upwelling index (UI intensity). Varela et al. (2015) demonstrated opposite results world wide depending on the length of data, season evaluated, and selected area within the same wind dataset or between datasets. For the Mauritanian region, when wind stress data were used (Varela et al., 2015), a more persistent increasing trend in upwelling-favourable winds north of 21ºN and a decreasing trend south of 19ºN was determined.

Starting in June 2005, the QUIMA-VOS line visited the Mauritanian-Cape Verde upwelling region northwest of Africa on a monthly basis (Fig. 1 and Supplementary Table S1) producing for the first time a high resolution database of SST and partial pressure of CO_2 expressed as fugacity fCO_2. This database shows the variations in the CO_2 system under changes in the upwelling conditions in the Canary Ecosystem from 27ºN to 10ºN for the period 2005 to 2012.

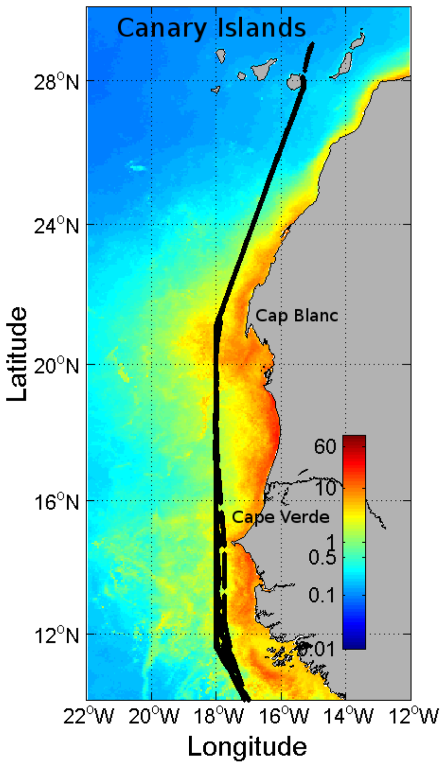

Fig. 1. Ship track in the area from 28ºN (Gran Canaria, The Canary Islands) to 10ºN (black dots). The locations of Cap Blanc and Cape Verde are indicated. Monthly Ocean Color (oceancolor.gsfc.nasa.gov) data for average chlorophyl *a* concentration (mg m^{-3}) were included in a MatlabTM routine and annually averaged. The map has been generated using Matlab 7.12 R2011a.

EXPERIMENTAL

2.1 Study Region.

The VOS line crosses the East Atlantic Ocean from the north of Europe (English Channel) to South Africa, calling at Gran Canaria, the Canary Islands, with a periodicity of two months, which provides monthly data (southward or northward sections). In this work, the area between Gran Canaria at 27ºN and 10 ºN has been selected in order to study the Mauritanean-Cape Verde upwelling region. In its route south (Fig. 1), the ship leaves Gran Canaria, and goes straight to 100 km off Cap Blanc, at 21ºN 17º45'W. It then follows this longitude, passing at 100 km off Cape Verde until 12ºN, where it changes direction to Cape Town, reaching 10ºN 17ºW at 330 km out of the coast of Guinea. Between 22ºN and 20ºN, the ship reaches the 500 m isobath. South of 15ºN, the ship moves between 1000 and 500 m isobath. In its route north, the ship follows the same reverse track.

2.2 Experimental data

Experimental data were obtained under the EU projects Carboocean and Carbochange (www.CarboOcean.org, https://carbochange.b.uib.no/) and now also available at http://www.socat.info/. An autonomous instrument for the determination of the partial pressure of CO_2 developed by Craig Neill following NOAA recommendations was installed in a VOS line. This was operated by the MSC company from 2005 to 2008 and the Maersk Company from 2010 to 2012. This VOS line (QUIMA-VOS) run between the UK and Cape Town, from July 2005 to January 2013 (Supplementary Table S1). Temperature was measured at three locations along the sampling circuit: in the intake (SeaBird SBE38L), in the equilibrator (SeaBird thermosalinograph SBE21 and internal PT100 thermometer), and in the oxygen sensor (Optode 3835 Aanderaa™). After the seawater pump, the intake is divided in two lines, one feeding the CO_2 system and the other the oxygen sensor, the fluorometer and the seabird thermosalinometer. Differences between equilibrator and intake were constant in time due to the high seawater flow but varied among ships due to the different locations of the equipment. Values varied between 0.06ºC when the equipment was placed close to the intake to 0.35ºC, when the equipment was one floor above, inside the engine room. The SST was also obtained from the NOAA_OI_SST-V2 data provided by the NOAA/OAR/ESRL PSD, Boulder, Colorado, USA (http://www.esrl.noaa.gov/psd). These data had a spatial resolution of 1º latitude and 1º longitude and monthly averages were used. The correlation between our experimental SST data and satellite one was better than ± 1ºC, and improved to ± 0.4ºC after removing the most affected upwelling regions (19-22ºN and 14-16ºN), related to the high variability imposed by the upwelling.

The CO_2 molar fraction, xCO_2, in seawater was obtained every 150 s, while atmospheric xCO_2 data were obtained every 180 min. The seawater intake was located at a 10 m depth. The system was calibrated every three hours, by measuring four different standard gases with mixing ratios in the ranges of 0.0, 250-290 ppm, 380-410 ppm and 490-530 ppm of CO_2 in the air, provided by NOAA and traceable to the World Meteorological Organisation scale. The precision of the system is greater than 0.5 µatm and the accuracy estimated with respect to the standard gases is of 1 µatm inside the standards range. For xCO_2 values higher than the highest standard (532.04 ppm), the accuracy will be reduced, even when linearity was observed in all cases inside the standards range. The fugacity of CO_2, fCO_2 (µatm), was calculated from xCO_2 after correcting for temperature differences between intake and equilibrator, according to the expressions for the seawater given by DOE (1994). Normalised fCO_2 to the mean SST for the area (T_{mean}) was computed following Takahashi et al. (1993)

$$(Nf\mathrm{CO_2}) = f\mathrm{CO_2} \cdot \exp[0.0423(\mathrm{T_{mean}} - \mathrm{SST})] \quad (1)$$

In order to compute a second carbonate system variable, the surface total alkalinity was computed from sea surface salinity (SSS) and SST (Lee et al., 2006). pH_T at the in situ temperature was computed from fCO_2 and A_T and with average annual surface ocean total phosphate and total silicate concentrations of 0.5 and 4.8 µmol kg^{-1}, respectively, from the World Ocean Atlas 2009, using the carbonic acid acidity constants by Merbach et al. (1973) refitted by Dickson and Millero (1987).

Air-sea CO_2 fluxes, FCO_2 (mmol m^{-2} d^{-1}), were evaluated as

$$FCO_2 = 0.24 * k * s * (fCO_2^{sw} - fCO_2^{atm}) \quad (2)$$

where 0.24 is the scale factor, *k* is the gas transfer velocity, *s* is the CO_2 solubility, fCO_2^{sw} is the seawater fugacity of CO_2 and fCO_2^{atm} is the atmospheric fugacity of CO_2. In order to evaluate (fCO_2^{sw} - fCO_2^{atm}), fCO_2^{atm} data were linearly interpolated to the fCO_2^{sw} time vector. A positive value for FCO_2 corresponds with a CO_2 outgassing from the ocean. *k* (cm h^{-1}) was evaluated with the parametrization (Nightingale et al., 2000):

$$k = (0.222 * W^2 + 0.333 * w) * (Sc/660)^{-1/2} \quad (3)$$

where *W* is the wind speed at 10 m above the sea surface (m s^{-1}) and *Sc* is the Schmidt number.

The variables involved in estimating FCO_2 data (i.e. fCO_2^{sw}, fCO_2^{atm}, SST and SSS) were fitted to sinusoidal expressions (Lüger et al., 2004) for a given latitude as:

$$X(lat)^* = a_0 + a_1(t - 2005) + a_2 sin(2\pi t) + a_3 cos(2\pi t) + a_4 sin(4\pi t) + a_5 cos(4\pi t) \quad (4)$$

where a_i are the fitting coefficients, t is the sampling time expressed as year fraction and X* represents any of the four fitted variables. This procedure allowed us to re-construct the series of experimental data for periods without monthly data. The variables were decomposed into an interannual term $X(lat)_t^* = a_0 + a_1(t - 2005)$ plus a periodical term $X(lat)_p^* = a_2 sin(2\pi t) + a_3 cos(2\pi t) + a_4 sin(4\pi t) + a_5 cos(4\pi t)$, that is, $X(lat)^* = X(lat)_t^* + X(lat)_p^*$. The periodical term accounts for the high frequency seasonal variability, while the interannual one marks the year-to-year trend. First, observations were grouped in a natural year for a given latitude, as if they had been taken in a single year (no correction was done for interannual variability). The mean seasonal climatology data associated with the periodic coefficients (i.e. a_2, a_3, a_4, and a_5) throughout the sampling period were determined. Next, the interannual coefficients a_1 were calculated by fitting the residuals resulting from subtracting the periodical component, $X(\mathrm{lat})_p^*$, from the original variable $X(lat)$. Fixing these five coefficients (a_1-a_5), new distributions for fCO_2^{sw*}, fCO_2^{atm*}, SST^* and SSS^* were constructed with a daily resolution based on the curve fits given for each variable as in Eq. (4), providing the coefficient a_0. The accuracy of this fitting procedure was checked by both computing the correlation between experimental and reconstructed values and by determining the mean residuals. The Pearson coefficients were always over 0.87 for SST (average 0.94 ± 0.03), over 0.69 for both fCO_2^{sw}, fCO_2^{atm} (average of 0.79 ± 0.07 and 0.82 ± 0.04, respectively) and over 0.67 for SSS (average 0.79 ± 0.07). The mean residual on the determination of those four variables were ± 3.7 µatm, ± 1.5 µatm, ± 0.22 ºC, and ± 0.05 for fCO_2^{sw*}, fCO_2^{atm*}, SST^* and SSS^*, respectively. When the monthly satellite SST values were considered, the new SST* function averaged for each month produced values within ± 0.47ºC, confirming that this procedure was able to fit non-sampled periods. It was assumed that the same procedure was valid for non-sampled fCO_2. Finally, daily FCO_2^*

time series between 10ºN and 27ºN with a latitudinal resolution of 0.5° were calculated with a standard error of estimation of 0.5 mmol $m^{-2} d^{-1}$ (15% of error) that produced mean residuals (experimental FCO_2 - FCO_2^*) of 0.4 mmol $m^{-2} d^{-1}$ and Pearson correlation coefficients between experimental and computed FCO_2^* of $r > 0.6$, $p < 0.01$.

Chlorophyll-a was calculated from measurements made by the Moderate Resolution Imaging Spectroradiometer (MODIS) aboard NASA's Aqua satellite. We used monthly averages with spatial resolution of 9 km supplied by Ocean Color (oceancolor.gsfc.nasa.gov).

Wind data were downloaded from the NCEP CFSR database at http://rda.ucar.edu/pub/cfsr.html developed by NOAA and retrieved from the NOAA National Operational Model Archive and Distribution System and maintained by the NOAA National Climatic Data Center. The spatial resolution is approximately 0.3 × 0.3° and the temporal resolution is 6 hours. The reference height for the wind data is 10 m.

Rainfall data were collected by the Precipitation Radar installed on the Tropical Rainfall Measuring Mission (TRMM) satellite (http://precip.gsfc.nasa.gov). Monthly averages with a spatial resolution of 0.5º×0.5º (product 3A12, version 07) were used (Supplementary Fig. S1) in order to explain changes in seasonal surface salinity distributions.

2. RESULTS AND DISCUSSION

3.1 Physical propeties

The variability of the Mauritanian-Cape Verde upwelling was analyzed in terms of the upwelling index (Nykjaer and Van Camp, 1994) (Fig. 2) using satellite wind data. Negative (positive) UI values correspond to upwelling (downwelling) favorable conditions. The strongest negative values of the index correspond to more intense upwelling. Results clearly distinguish two main subareas in the upwelling system.

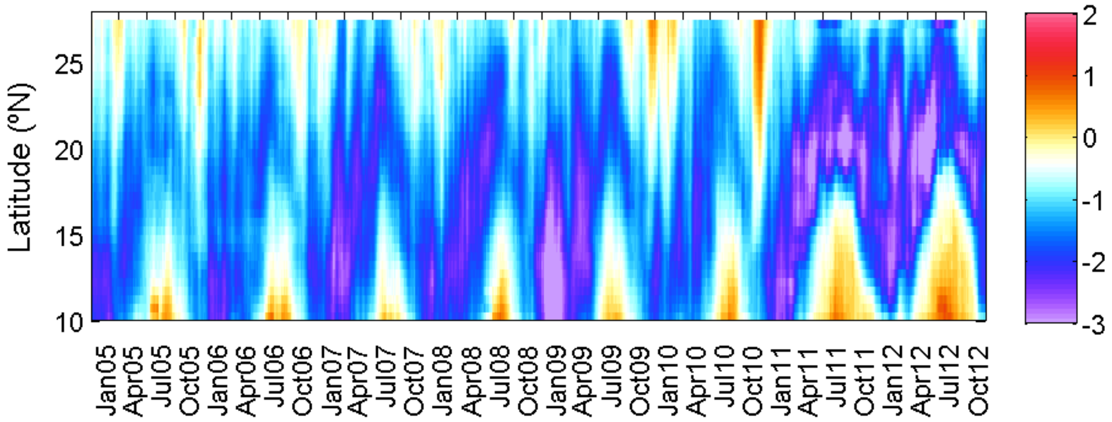

Fig. 2. Time series of upwelling index (UI*10^{-3} m^2 s^{-1}) in the Mauritanian-Cape Verde upwelling region along the ship track computed following Nykjaer and Van Camp (1994). Cool colours are related to upwelling events and warm colours to downwelling events.

1) North of 20ºN, the upwelling conditions were favorable throughout the year, although the highest upwellings were observed from March to September with a northward shift from 20º to 22ºN. 2) South of 20ºN, a marked seasonality was observed with favorable upwelling conditions during autumn and winter, with the maximum intensity observed during January and February. In this region, a downwelling regime is present between May and November when the summer trade winds are replaced by the monsoonal winds advecting warm water (Fig. 3a) northward along the shore (Nykjaer and Van Camp, 1994).

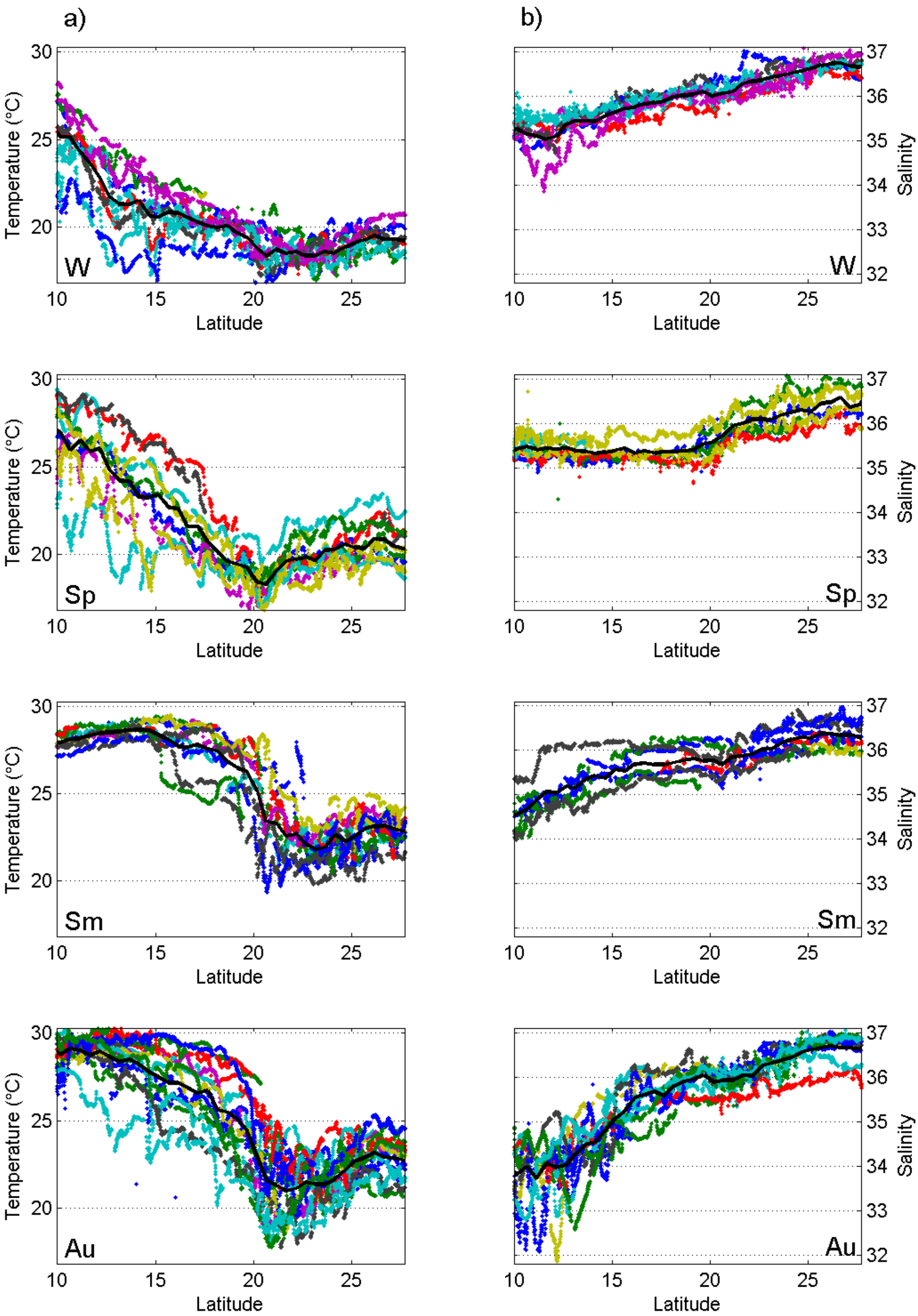

Fig. 3. *In situ* data of a) SST and b) SSS data in the Mauritanian - Cape Verde coastal region grouped by seasons: winter (W, December, January and February), spring (Sp, March, April and May), summer (Sm, June, July and August) and autumn (Au, September, October and November). The averaged values for all cruises in Table S1, are shown in black for each season including the 95% confidence limits. Colour code for each cruise is that indicated in Table S1.

Our results (Fig. 2) are quite consistent with previous research (Nykjaer and Van Camp, 1994; Marcello et al., 2011; Santos et al., 2005; 2012; Cropper et al., 2014) but include the years 2010 to 2012 where UI at around 20-21ºN presented a shift of the upwelling regime intensity from high (-2000 m^2 s^{-1}) to strong (-2800 m^2 s^{-1}). The analysis of upwelling trends along this area has been controversial since it is highly dependent on the selected region (Santos et al., 2012). The inter-annual evolution of UI over the period 2005 to 2012 (Fig. 4, green line) for each degree in latitude, iindicates an increase in the UI (mean confidence interval of 9 m^2 s^{-1}) as showed by Santos et al. (2012).

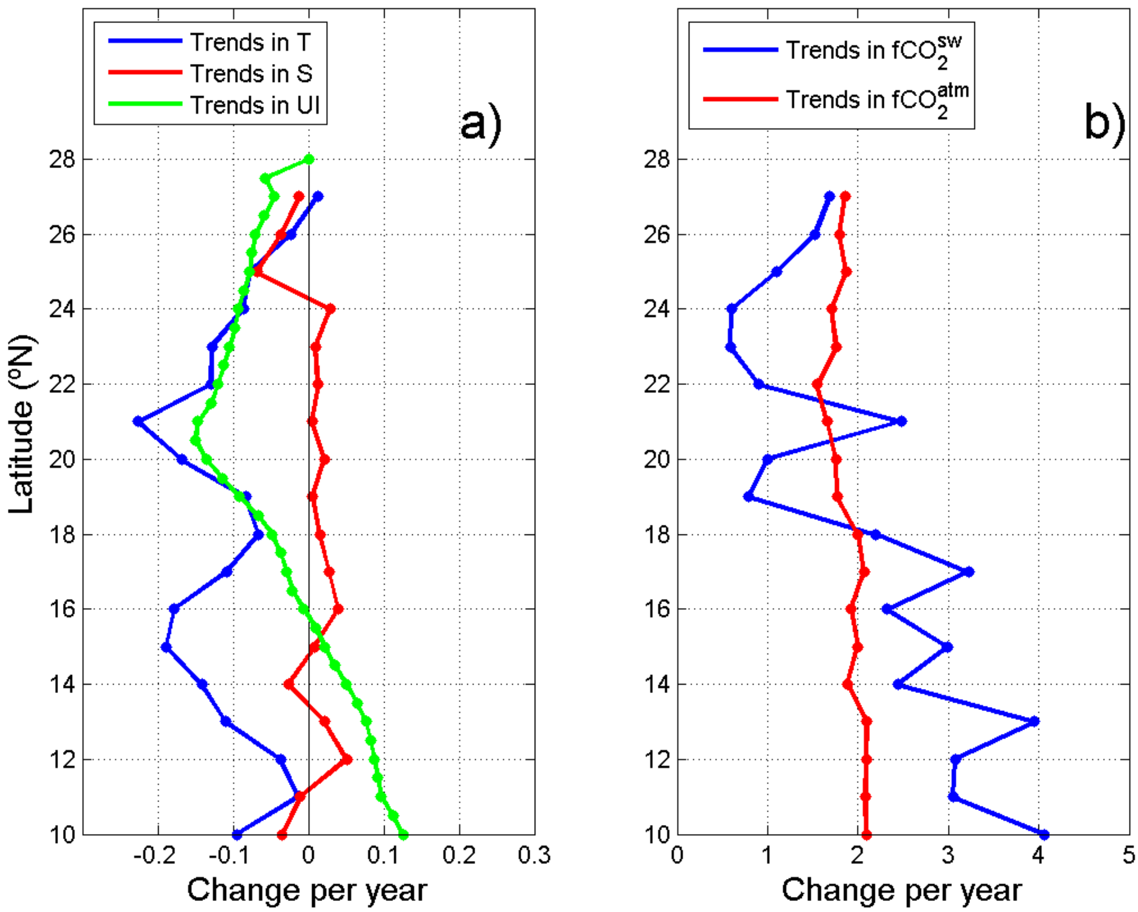

Fig. 4. Latitudinal distribution of the interannual trends for the Upwelling Index (UI*10^{-3}) and for the four experimental variables along the QUIMA-VOS line integrated over every degree between 2005 and 2012. The a) panel presents the trends for Upwelling index (UI*10^{-3} m^2 s^{-1}, mean confidence interval of 9 m^2 s^{-1}), SST (ºC yr^{-1}, confidence interval 0.13ºC) and SSS (yr^{-1}, confidence interval 0.06) and the b) panel the trends for fCO_2^{sw} and fCO_2^{atm} (confidence intervals 4.23 µatm and 0.44 µatm).

North of 15ºN, the upwelling index confirmed the stronger upwelling observed since 1995-1996 in this region after a more than a 10-year (from at least 1982 to 1995) period of weaker upwelling (Santos et al., 2012). Local zonal differences between ocean and coastal SST trends determined with satellite data confirmed the intensification of the upwelling regime along the African coast for the period 1982 to 2000 (Santos et al., 2005) extended by Santos et al. (2012) until 2010, and extended in this study until 2012 (data not shown). This has been described as a decadal scale shift of the upwelling regime intensity (Marcello et al., 2011; Santos et al., 2012).

South of 15ºN, the annual UI values and trends (Fig. 2 and 4) both for the upwelling (values close to -2800 m^2 s^{-1} in January) and downwelling (values reaching 1850 m^2 s^{-1} in July) periods are becoming stronger. At 11-12N, were downwelling is becoming stronger, this results in negative annual temperature rates that appraches to zero. The UI index serves as an indication of decadal variability of the summer monsoon winds and associated northward advection of warm water along the coast (Santos et al., 2012).

The highest upwelling intensity along the VOS line was located at the capes, Cap Blanc and Cape Verde. From satellite chlorophyll-*a* data, especially off Cap Blanc, giant filaments with chlorophyll concentrations above 1 mg m^{-3} persist year-round, spreading from the coast several hundred kilometers offshore (Fig. 1). North of Cap Blanc the upwelled water originates from the North Atlantic Central Water, and mixes with South Atlantic Central Water, SACW, towards the south (Mittelstaedt, 1983). South of Cap Blanc, the upwelling of nutrient rich SACW (Mittelstaedt, 1983) promotes phytoplankton growth between Cap Blanc and Cape Verde. Towards 12°N, upwelling is also fed by the North Equatorial Under Current (Hagen and Schemainda, 1984). Moreover, the entire northwest African coast is also influenced by the African desert dust transport by the mid-tropospheric Harmattan winds originating from the central Sahara, which supplements the levels of micronutrients (such as iron) to the adjacent marine ecosystem (Mittelstaedt, 1983*;* Neuer et al., 2004).

The study area is also affected by the migration of the Inter-Tropical Convergence Zone (ITCZ), related to maximum precipitation rates (Hastenrath, 1995). To have a significant satellite precipitation record in our region of interest, precipitation data were integrated longitudinally between 25.25ºW and 9.75ºW. Time series for the latitudinal distribution of integrated precipitation (Supplementary Fig. S1) identified the average position of the ITCZ related to maximum precipitation rates. The ITCZ was located at its southernmost position (2ºN) during winter, reaching its northernmost position (14-16ºN) around summer. The ITCZ reached our area of interest (>10°N) from late spring to late summer.

The latitudinal distributions of measured SST and SSS along the vessel track are shown in Fig. 3, grouped by seasons. The temperature generally decreased from 10ºN to about 20ºN to 21ºN, where the ship meets the Mauritanian upwelling. From there to the north, the temperature rises as the ship leaves the upwelling area on its way to the Canary Islands. In situ temperature at 27°N shows temperatures in the range of 18 to 24°C with the minimum in winter and maximum in late summer-early autumn. The annual temperature range was somewhat higher at 20°N, with summer maximum of around 26°C and minimum in spring of about 17ºC. At 10°N, temperatures were the highest throughout the year (>25°C), with minimum values in winter and maximum in late spring and late autumn. The low values observed during the end of summer are related to the arrival of the ITZC (Supplementary Fig. S1) at those latitudes. The thermal distribution shows a temperature increase as we move to the Equator and a notable cooling at the upwelled waters off Mauritania. Only during winter time and the begining of the spring, the upwelling of cold water from Cape Verde area was detected. Salinity minimum values were normally located at 10ºN, increasing to maximum values at the Canaries' latitude.

The minimum values of salinity were exceptionally low during autumn from 10ºN to 16ºN by both the freshwater input from rivers that increase their outflow during this season (Nicholson, 1981) and by the northward shift of the ITCZ during this part of the year.

Anomaly fields for temperature and salinity (data not shown) were calculated as the difference between the observations and the mean values at each season for individual latitudes. For temperature, the largest anomalies in winter and spring were located south of 18°N, with values of ±2ºC, related to the seasonal cycle of the Cape Verde upwelling. During summer the pattern changed and the largest anomalies were detected in the upwelling area at 18-22°N, with values of ±5ºC when the upwelling index for the Mauritanian area was highest (Fig. 2). In autumn the temperature anomalies were shifted slightly to the north, 20-24°N, with values of ±3ºC related to the observed pulses in upwelling favorable winds that affected the surface seawater properties. On the other hand, salinity anomalies showed a very homogeneous pattern in all latitudes for winter, spring and summer, with values generally within ±0.5. However, during autumn important anomalies south of 18°N were observed, with values in the range of ±1.5. In this region, the upwelling development, the river discharge and the rainy season controlled the observed distribution (Yoo and Carton, 1990).

The data conclude a permanent annual upwelling regime observed north of 20ºN and a seasonal regime across 10–19ºN, in accordance with the climatology of previous studies. The data confirm also an increase in upwelling conditions north of 20ºN and an increase in downwelling conditions south of 20ºN.

3.2 Carbon dioxide variability

The latitudinal distribution of the seasonal fCO_2^{sw} data (Fig. 5a) showed the highest values between 18 and 23ºN for all seasons due to the variability imposed by the upwelling off Mauritania. fCO_2^{sw} was consintently greater than the fCO_2^{atm}. During winter, when the Cape Verde upwelling develops (Fig. 2), the 12-15ºN region also presented higher fCO_2^{sw} values than those in the atmosphere. fCO_2^{sw} data showed a latitudinal shift between the seasons following the shift observed in the upwelling index: i.e., in winter, the largest values were located between 19º and 24ºN; in spring, they were located between 16º and 22ºN; during summer and autumn, the largest fCO_2^{sw} values were recorded in the range 20º to 23ºN. The difference between fCO_2^{sw} normalized to the mean SST of 22ºC for the region ($NfCO_2^{sw}$) and fCO_2^{sw} (ΔfCO_2, Fig. 5b) reinforced the variability at 20-23ºN all year around and at 12-17ºN during winter and spring, indicating that upwelling is the major factor contributing to the fCO_2 variability.

According to Takahashi et al. (1993), fCO_2^{sw} increases with temperature at a rate of 4.3% µatm ºC^{-1} (between 15 and 26 µatm ºC^{-1} in this area) in a thermodynamically controlled system. At 27ºN, as SST increases, the rate was only of 7.45 µatm ºC^{-1} due mainly to biological uptake and also to the CO_2 outflux. At 20ºN the rate became negative with a value of -10.9 µatm ºC^{-1}, clearly indicating the important injection of cool and CO_2 rich seawater at the upwelling area. The injection is not being compensated by the solubility nor the biological carbon pumps. At 10ºN, the rate was still negative, but only -4.3 µatm ºC^{-1} as a result of the seasonal upwelling. $NfCO_2^{sw}$ was related with SST (data not shown) in order to account for effects not removed during normalization. At latitudes 19º to 21ºN, in the upwelling vicinity of Cap Blanc, an inverse relationship of 70-100 µatm ºC^{-1} was found during winter and spring, while in summer and autumn the

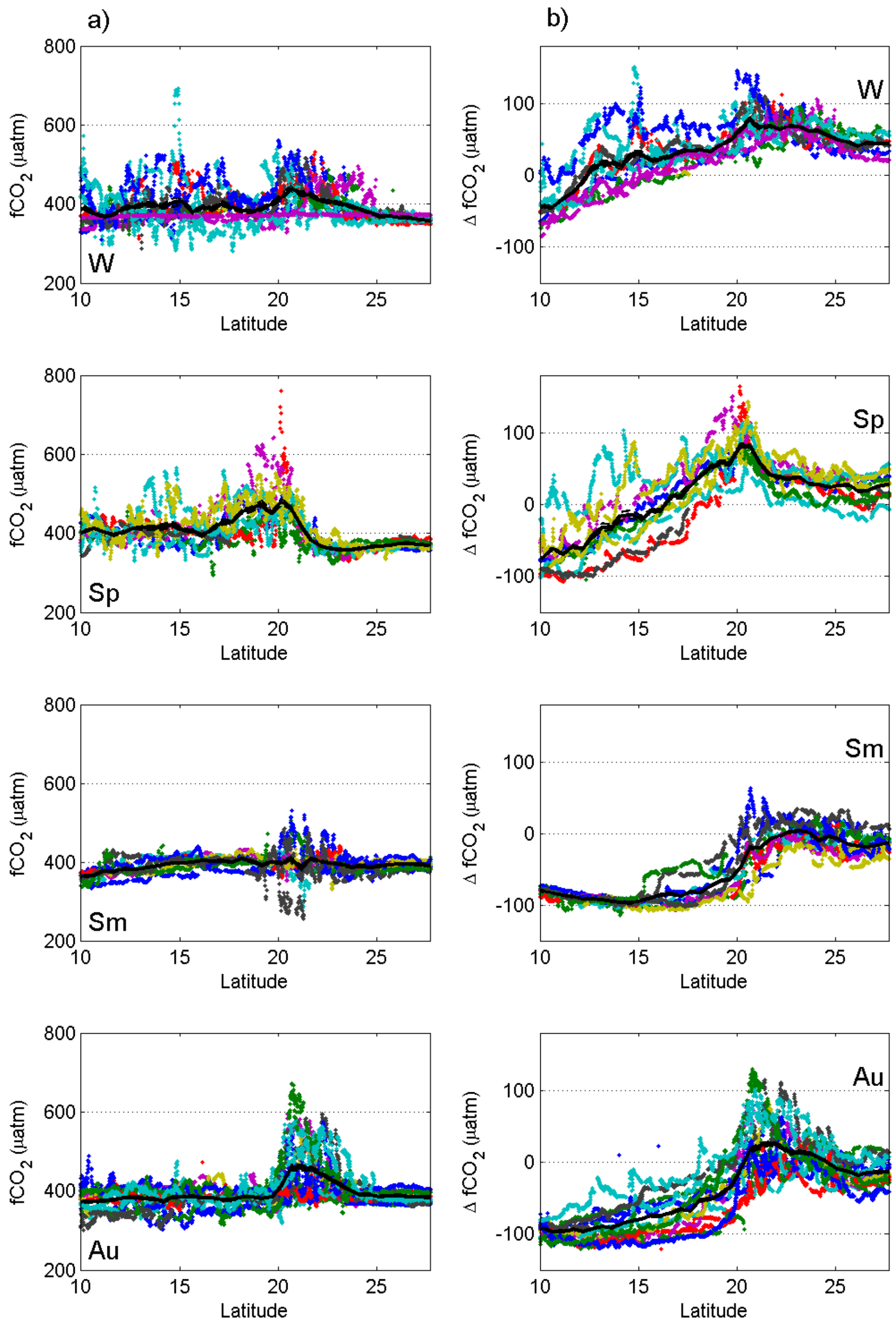

Fig 5. Fugacity of CO_2 data in the Mauritanian-Cape Verde coastal region grouped by seasons: winter (W, December, January and February), spring (Sp, March, April and May), summer (Sm, June, July and August) and autumn (Au, September, October and November). a) fCO_2^{sw} latitudinal distribution. b) Difference between measured and Normalized fCO_2^{sw} values to a constant temperature of 22ºC. The averaged values for all cruises in Table S1, are shown in black for each season including the 95% confidence limits. Colour code for each cruise is that indicated in Table S1.

inverse relationship was reduced to 12-18 μatm ºC^{-1}. While the upwelling indexes at those latitudes were quite constant throughout the year, different rates observed should be related to biological consumption of the CO_2 excess. However, during winter and spring the injection of CO_2 in the upwelling is not decreased by the biological activity in the area. But during the Chl-*a* maximum (late spring and summer) most of the CO_2 was consumed and/or exported and, therefore, the rate was strongly reduced.

Figure 4 depicts the observed interannual trends (a_1 coefficient in Eq. 4) for the four experimentally recorded detrended parameters, together with the UI trend. Confidence intervals of the computed mean annual values for SST, SSS, fCO_2^{atm}, fCO_2^{sw} were 0.13ºC, 0.06, 0.44 μatm and 4.23 μatm, respectively. There was a clear SST trend whereby seawater along the VOS line track was getting cooler with maximum cooling rates at the location of Cap Blanc (21ºN) and Cape Verde upwellings (15ºN) with rates higher than -0.2ºC yr^{-1}. Data from the first three years (2005 to 2008) at 21ºN showed lower temperatures with higher cooling rates that reached -0.7ºC yr^{-1}, although three years of data are not representative. The area crossed by the VOS line along 17º45'W from 22ºN to 10ºN is located inside the 1000 m isobath that is well inside the mean frontal activity in the Canary region, about 200 km wide (Wang et al., 2015). The different changes in temperature in the coastal slope and offshore waters are related to the different origins of the waters upwelled from depths of about 100 m to the surface (Mittelstaedt, 1983) that spread off the coastal area. The offshore water SST is less variable owing to longer residence time in the ocean surface. These effects and the fact that the VOS line keeps a track line that crossed the upwelling cells at a distance to the coast that varies among cells, contributes to the observed spatial variability. There was no attempt to compare latitudinal and longitudinal effects on the observed values. Our experimental data, however, does not show any positive SST rates in the upwelling affected area, and only when the ship approached the Canary Islands, the trends became less negative, reaching a value of +0.02ºC yr^{-1} at 27ºN, similar to those obtained for oceanic Atlantic water (Bates et al., 2014).

fCO_2^{atm} for the area presented the interannual increase of about 2 ± 0.3 μatm yrr^{-1} observed in atmospheric stations, while fCO_2^{sw} presented a heterogeneous distribution. South of 18ºN the rate of increase was always higher than that in the atmosphere reaching a maximum value of 4.1 ± 0.4 μatm yr^{-1} at 10ºN. At 27°N, fCO_2^{sw} increased at a rate of 1.7 ± 0.2 μatm yr^{-1} similar to that determined at the ESTOC time series site (González-Dávila et al., 2010) located at 29º10' N 15º30'W. In the Cap Blanc area, fCO_2^{sw} increased at an average rate of 2.5 ± 0.4 μatm yr^{-1} with the highest values in the period 2005 to 2008 (a rate of 4.6 ± 0.5 μatm yr^{-1} was computed with only those years). Around Cap Blanc, fCO_2^{sw} always presented lower rates of increase than in the atmosphere with values well below 1 μatm yr^{-1}. The observed decrease in SST and the trends in fCO_2^{sw} can only be explained by a reinforced upwelling. North of 18ºN, the lowest rate of increase in fCO_2^{sw} compared to fCO_2^{atm}, together with a decrease in temperature, indicated that upwelling is also favoring an increase in the net community production around the Mauritanian upwelling, consuming and/or exporting the CO_2 rich upwelled waters favored by the lateral transport of the Mauritanian current (Lachkar and Gruber, 2013; Varela et al., 2015). The upwelling intensification effects observed in the trends of our experimental data support the recent wind stress trends (Crooper et al., 2014; Varela et al., 2015; Santos et al., 2012) of increased upwelling-favorable winds, at least for the period 2005-2012 in the Canary upwelling region (Fig. 2 and 4). The intensification of the upwelling results in a change in the measured upwelled water properties due to either higher upwelling velocities or deeper source upwelled waters. However, what remains unclear from these records is to what extent those changes reflect upwelling variations due to climate change forcing versus natural decadal variability in the upwelling areas occurring over interannual timescales.

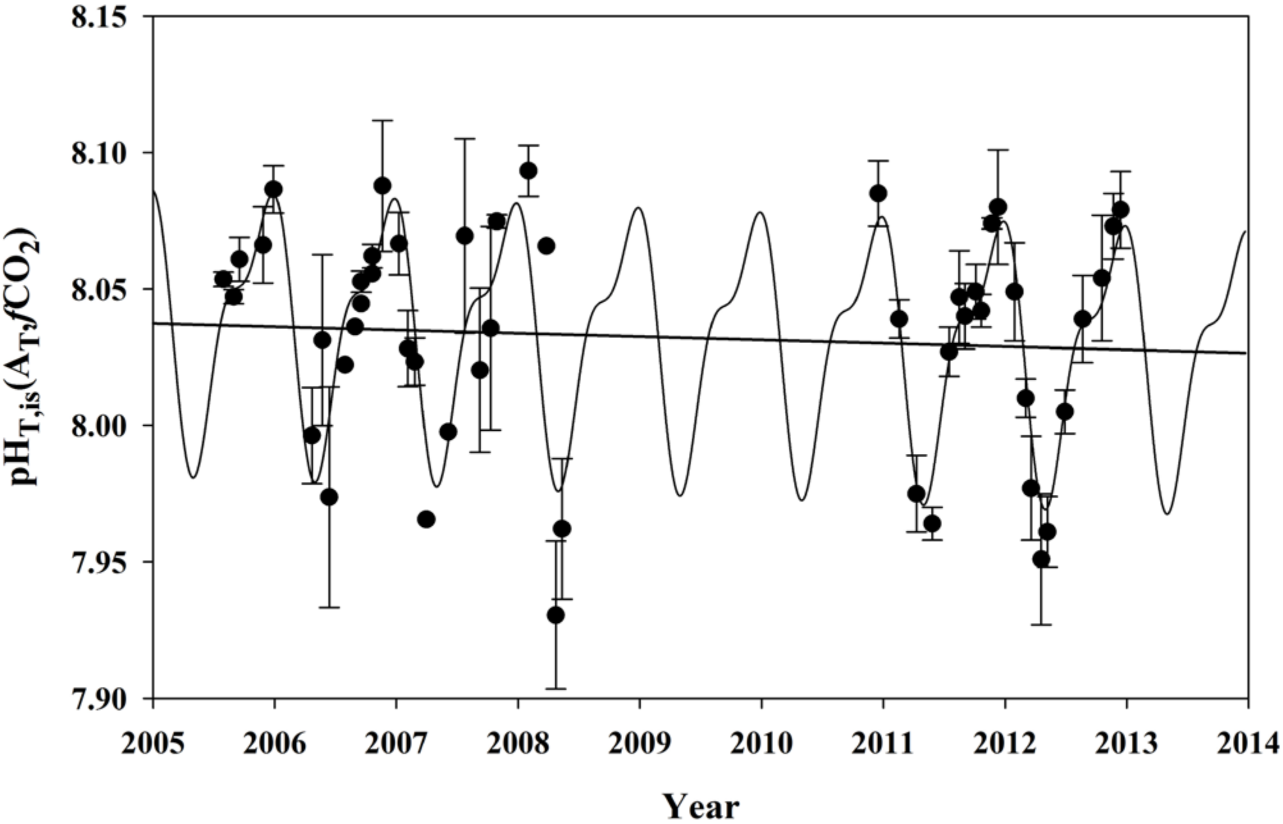

Fig. 6. pH at *in situ* SST in total proton scale computed from total alkalinity (based on regional correlations with SST and SSS, Lee et al., 2006) and fCO_2 at 21 ± 0.25 ºN. The error bar represents the standard deviation of the computed data for each cruise for the selected latitude. The black line shows the harmonic fitting Eq. (4) for the data and the corresponding linear trend.

Because the upwelling intensity is changing, other variables will also be affected. $pH_{T,is}$ at 21 ± 0.25ºN was computed from fCO_2 and alkalinity pairs of data. Alkalinity was computed from regional correlations with SST and SSS (Lee et al., 2006) which could under-represent seasonal and interannual variations in upwelling areas. However, pH computed from fCO_2 values are relatively insensitive to errors in $A_{T,}$ and fCO_2 controls the magnitude and variability of pH (a 60 µmol kg^{-1} change in A_T will affect a 0.1% in pH, that is, about 0.01 pH units). Figure 6 depicts the computed $pH_{T,is}(A_T, fCO_2)$ data and the harmonic fitting Eq. (4) providing seasonal variability and interannual trend. Considering the small systematic biases in interannual dynamics, we determined a decrease in pH at a rate of -0.003 ± 0.001 per year (Fig. 6). This decrease is one of the highest rate values determined in several time series stations (Bates et al., 2014), where oceanic SST has only slightly increased in the last decades. However, at the Mauritanian upwelling area and at the location where our VOS line approached this region, SST decreased at a rate of -0.22 ± 0.06ºC yr^{-1} (Fig. 4). Solely, this decrease in temperature would increase the pH by a rate of +0.004 yr^{-1} and the fCO_2 would decrease by 4 µatm yr^{-1}. The net effect of the increase in the amount of rich CO_2/low pH upwelled waters in the Mauritanian upwelling would be, therefore, a decrease in the pH of over -0.007±0.002 units yr^{-1} and an increase in fCO_2 of +6.5 ± 0.7 µatm yr^{-1} (with periods where those rates could reach values of 0.015 yr^{-1} in pH and 10.5 µatm y^{-1} in fCO_2 as recorded during 2005-2008). Those values are greatly compensated by the important decrease in the SST resulting in the determined rates of -0.003 ± 0.001 pH units and +2.5 ± 0.4 µatm of fCO_2 per year.

This new data set of experimental values confirmed a decrease in SST and trends in fCO_2^{sw} than can only be explained by a reinforced upwelling conditions, that favor an increase in the net community production around the Mauritanian upwelling together with a more corrosive environment with pH values that decrease by over -0.007±0.002 units at 21ºN. However, the decrease in SST in the upwelling cell buffers this rate to values around -0.003 ± 0.001 pH units yr^{-1} and +2.5 ± 0.4 µatm yr^{-1} in fCO_2, still among the highest observed in other time series.

3.3 Fluxes of CO_2

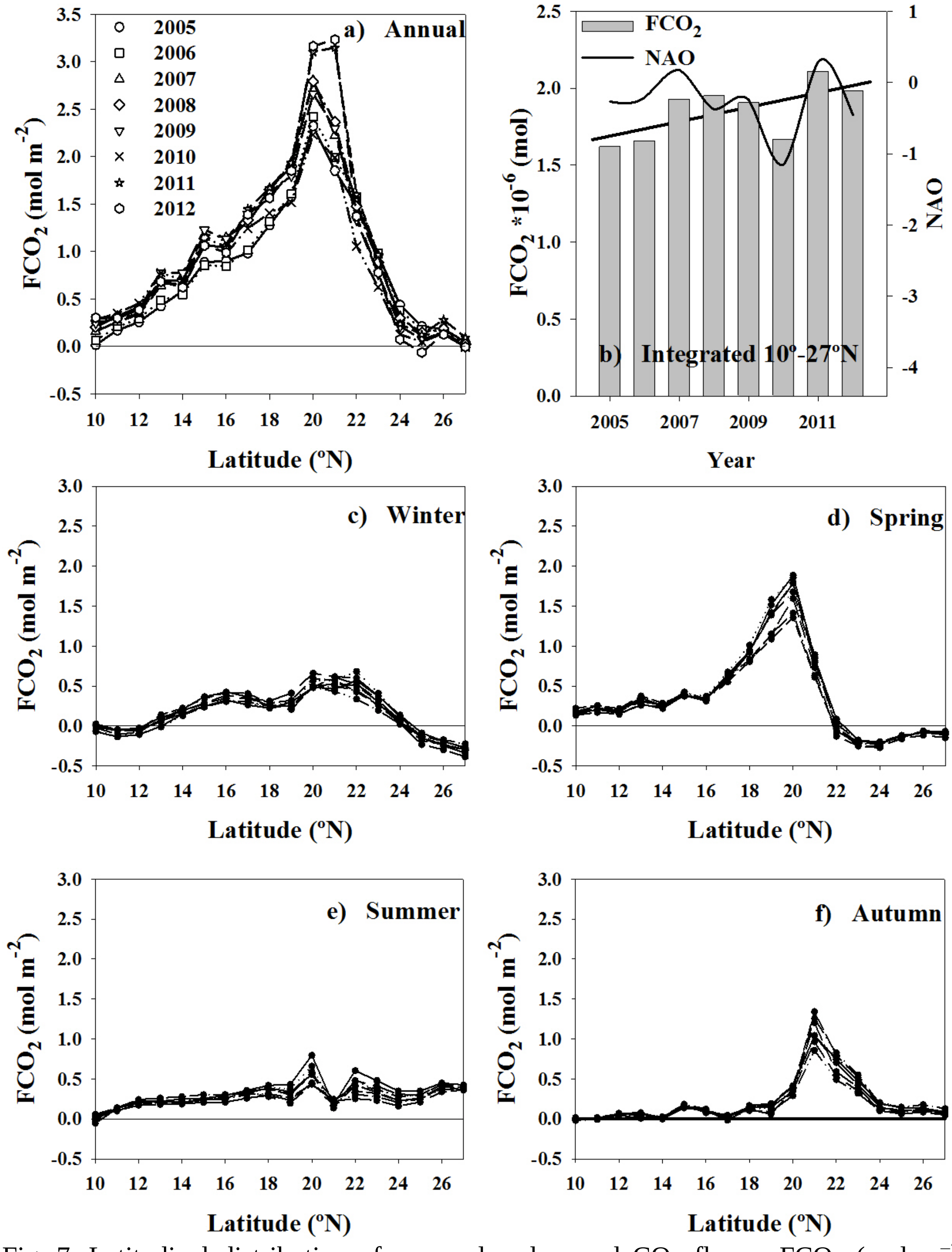

Fig. 7. Latitudinal distribution of seasonal and annual CO_2 fluxes, FCO_2 (mol m^{-2}). Fluxes of CO_2 were computed using Nightingale et al. (2000) parametrization and satellite winds with a resolution of 6 hours. a) Integrated year-to-year from 2005 to 2012 and b) latitudinally integrated for 2005 to 2012 together with annual values for NAO index. Latitudinal distribution of FCO_2 seasonally integrated from 2005 to 2012 are depicted for winter (c, December, January and February), spring (d, March, April and May), summer (e, June, July and August) and autumn (f, September, October and November).

The annual air-sea CO_2 flux for the full domain was positive (Fig. 7a), with the area off with values close to 3.3 mol CO_2 m^{-2} (Fig. 7a). North of 24ºN, in the area not affected by the coastal upwelling, an average flux of +0.14 ± 0.03 mol CO_2 m^{-2} was determined. The ingassing observed during winter and spring of -0.16 ± 0.03 mol CO_2 m^{-2} for the full period (Fig. 7) was surpassed by the outgassing during summer and autumn of 0.28 ± 0.14 mol CO_2 m^{-2}. South of 24ºN, it was observed that during spring (Fig. 7d) the photosynthetic activity was not intense enough to uptake the CO_2 injected by the strongest upwelling in the surface waters and thus the area acted as a source of CO_2 with values reaching 1.9 mol CO_2 m^{-2} in 2012. During summer (Fig. 7e), primary producers and lateral advection of warm waters by the Mauritanian current could consume/export the CO_2 rich waters reaching values of 0.5 mol m^{-2}. During autumn (Fig. 7f), only the area between 20ºN and 23ºN acted as a source of 1-1.5 mol CO_2 m^{-2}, while the rest was almost in equilibrium. Late autumn-winter upwelling in the 14º to 17ºN region contributed to an increased outgassing with a second annual submaximum of about 0.4 mol CO_2 m^{-2} in winter (Fig. 7c). South of 14ºN, annual CO_2 fluxes decreased from about 0.7 mol m^{-2} at 14ºN to being roughly in equilibrium at 10°N.

The integrated CO_2 fluxes for the area 10ºN to 27ºN along the VOS line section for the years 2005 to 2012 (Fig. 7b) were between 1.6 and 2.1 10^6 mol, with an important annual variability. FCO_2 increased during the studied period by $0.05 \pm 0.02 \cdot 10^6$ mol yr^{-1}. The augment in FCO_2 is related to the observed increase in wind speed (Fig. 4, indicated as UI) north of 16ºN. North of 19ºN, the influence of wind speed far surpassed the effect of the smaller annual rate of increase in fCO_2^{sw} relative to fCO_2^{atm}, with an exception at 21ºN (Fig. 4). South of 16ºN, the decrease in wind speed did not exceed the effect of the incremental change in (fCO_2^{sw} - fCO_2^{atm}) associated with the increased downwelling indexes (Fig. 4; Santos et al., 2012), resulting in a slightly increasing FCO_2. The variability observed in the annual integrated CO_2 fluxes (Fig. 7b) was related with the basin-scale oscillations, the North Atlantic Oscillation (NAO) index and the East-Atlantic Pattern (EA) (http://www.cpc.ncep.noaa.Gov/data/teledoc/ telecontents.shtml). Cropper et al. (2014) found winter upwelling variability was strongly correlated with the winter NAO (r values ranged from 0.50 at 12–19ºN to 0.59 at 21–26ºN), due to the influence of the Azores semi-permanent high-pressure system on the strength of the trade winds. The annual integrated FCO_2 was related with the annual NAO index (Fig. 7b) with a similar r = 0.54, even when fluxes are not only controlled by wind strength. However, Fig. 7a clearly indicates that the Mauritanian upwelling area was the most important contributor to FCO_2 in the study area. The FCO_2 was not significantly correlated with the winter NAO (r = 0.23). Also, the EA index, which represents a southward-shifted NAO-like oscillation, presented a lower significant value (r = 0.48) (trends not shown), in agreement with the upwelling index (Cropper et al., 2014). Overall, the correlation between fluxes and climate indexes describing the main mode of variability across the Atlantic sector may be directly related to the Azores High and its influence on the trade wind strength.

FCO_2 values along the QUIMA-VOS line were used in order to compute a flux budget for the Mauritanean-Cape Verde region. The observed values were assumed to be valid for at least 100 km to both sides of the QUIMA-VOS line. In this case, the total flux of CO_2 being ejected to the atmosphere would reach a value of 16 Tg of carbon dioxide a year for the period 2005-2012, with a rate of increase of 0.6 Tg yr^{-1}. However, it should be considered that the export of the rich fCO_2 upwelled water with high nutrient concentration off the coastal areas would promote a decrease in surface fCO_2 values during productive seasons (as those observed north and south 21ºN) that will result in an ingassing of CO_2. This could balance the observed outgassing increase in a more global scale.

4. CONCLUSIONS

The Mauritanian-Cape Verde upwelling area's sensitivity to climatic forcing on upwelling processes strongly affects the CO_2 surface distribution, ocean acidification rates and air-sea CO_2 exchange.

The experimental SST and carbon dioxide system variables results for the period 2005 to 2012 confirm upwelling intensification at the Mauritanian-Cape Verde upwelling system. Furthermore, we have shown that upwelling regions at low-mid latitudes are important sources of CO_2 to the atmosphere. As a direct result, the pH is decreasing at a rate of -0.003 ± 0.001 per year. Importantly, the amount of emitted CO_2 is increasing annualy at a rate of 0.6 Tg due to stronger wind stress, even when primary production seems to also be enhanced in the upwelling area. The montly record in this EBUS is not yet long enough to determine the extent to which these changes can be attributed to natural decadal variability. These VOS line must be maintained for years to come, and will continue to be on of the most significat contributors to our knowledge of how ocean surface waters are being affected by present and future climate change. The results from VOS lines can provide accurate data for changes in SST, FCO_2 and, consequently, upwelling intensification effects due to global change conditions under decadal natural variability.

Data availability.

All data are free available at the SOCAT data base, http://www.socat.info/ and at the Carboocean and Carbochange web pages www.CarboOcean.org, https://carbochange.b.uib.no/, respectively

Team List

Melchor Gonzalez Davila, Professor of Marine Chemistry at the University of Las Palmas de Gran Canaria. Melchor.gonzalez@ulpgc.es

J. Magdalena Santana Casiano, Professor of Chemical Oceanography at the University of Las Palmas de Gran Canaria. Magdalena.santana@ulpgc.es

Francisco Machin, Associated Professor of Physical Oceanography at the University of Las Palmas de Gran Canaria. Francisco.machin@ulpgc.es

Author contributions

M.G.D. and J.M.S.C worked in the equipment installation, data collection and designed the study. F.M. processed the data, generated figures and results. All of them collaborated in the discussion of the data and the writing of the paper.

Competing interests

There is not any competing interest.

Acknowledgements

Financial support from the European Union through the Integrated Project FP6 CarboOcean under grant agreement no. 511106-2, FP7 project CARBOCHANGE under grant agreement no. 264879 and H2020 project ATLANTOS under agreement no.

633211 are gratefully acknowledged. Special thanks go to the Mediterranean Shipping Company (MSC) (years 2005- 2008) and the Maersk Company (years 2010-2013) who provided the ship platforms and scientific facilities. We thanks A. Abbott (Macquarie University, Sydney) for her comments and english correction. The Modis-Aqua Ocean Color Data, 2005-2012 reprocessing, NASA OB.DAAC, Greenbelt, MD, USA is strongly acknowledged.

References

Astor, Y., Scranton, M., Muller-Karger, F., Bohrer, R. N., and Garcia, J.: CO_2 variability at the CARIACO tropical coastal upwelling time series station, Mar. Chem., 97(3), 245–261, 2005.

Bakun, A.: Global climate change and intensification of coastal ocean upwelling, Science, 247(4939), 198–201, 1990.

Barton, E. D., Field, D.B., and Roy, C.: Canary current upwelling: More or less?, Prog. Oceanogr., 116, 167-178, 2013.

Bates, N. R., Astor, Y. M., Church, M. J., Currie, K., Dore, J. E., González-Dávila, M., Lorenzoni, L., Muller-Karger, F., Olafsson, J., and Santana-Casiano, J. M.: A time-series view of changing ocean chemistry due to ocean uptake of anthropogenic CO_2 and ocean acidification, Oceanography **27**(1), 126–141, doi:10.5670/oceanog.2014.16, 2014.

Borges, A. V., and Frankignoulle, M.: Distribution of surface carbon dioxide and air-sea exchange in the upwelling system off the Galician coast, Global Biogeochem. Cycles, 16(2), 1020, doi:10.1029/2000GB001385, 2002.

Borges, A. V., Delille, B., and Frankignoulle, M.: Budgeting sinks and sources of CO_2 in the coastal ocean: Diversity of ecosystems counts, Geophys. Res. Letters, 32, L14601, doi:10.1029/2005GL023053, 2005.

Cai, W.-J., Dai, M.,Wang, Y.: Air–sea exchange of carbon dioxide in oceanmargins: aprovince-based synthesis, Geophys. Res. Lett., 33, L12603, doi:10.1029/2006GL026219, 2006.

Chen, C. T. - A., Huang, T. –H., Chen, Y. C., Bai, Y., He, X., and Kang, Y.: Air-sea exchanges of CO_2 in the world’s coastal seas, Biogeosciences, 10, 6509-6544, doi:10.5194/bg-10-6509-2013, 2013.

Cropper, T. E., Hanna, E., and Bigg, G. R.: Spatial and temporal seasonal trends in coastal upwelling off NorthwestAfrica,1981–2012, Deep-Sea Res. I, 86, 94–111, 2014.

Demarcq, H.: Trends in primary production, sea surface temperature and wind in upwelling systems (1998–2007), Prog. Oceanogr., 83, 376–385, doi:10.1016/j.pocean.2009.07.022, 2009.

Dickson, A. G., Millero, F. J.: A comparison of the equilibrium constants for the dissociation of carbonic acid in seawater media, Deep-Sea Res., 34, 1733–1743, 1987.

DOE. Handbook of methods for the analysis of the various parameters of the carbon dioxide system in sea water, ORNL/CDIAC-74, http://cdiac.ornl.gov/oceans/handbook.html, 1994 (date of access 07/03/2017)

Dore, J. E., Lukas, R. , Sadler, D. W., and Karl, D. M.: Climate-driven changes to the atmospheric CO2 sink in the subtropical North Pacific Ocean, Nature, 424(6950), 754–757, 2003.

Feely, R. A., Boutin, J., Cosca, C. E., Dandonneau, Y., Etcheto, J., Inoue, H. Y., Ishii, M., Quéré, C. L., Mackey, D. J., McPhaden, M., Metzl, N., Poisson, A., and Wanninkhof, R.: Seasonal and interannual variability of CO_2 in the equatorial Pacific, Deep Sea Res. II, 49(13), 2443–2469, 2002.

Feely, R.A., Sabine, C. L., Hernandez-Ayon, J.M., Ianson, D., and Hales, B.: Evidence for upwelling of corrosive ‘acidified’ water onto the continental shelf, Science, 320 (5882), 1490–1492, doi:10.1126/science.1155676, 2008.

Frankignoulle, M., and Borges, A. V.: European continental shelf as a significant sink for atmospheric carbon dioxide, Global Biogeochem. Cycles, 15(3), 569–576, 2001.

Friederich, G. E., Ledesma, J., Ulloa, O., and Chavez, F. P.: Air-sea carbon dioxide fluxes in the coastal southeastern tropical Pacific, Prog. Oceanogr., 79(2-4), 156 – 166, 2008.

González Dávila, M., Santana-Casiano, M. J., Merlivat, L., Barbero-Munoz, L., and Dafner, E.: Fluxes of CO_2 between the atmosphere and the ocean during the POMME project in the northeast Atlantic Ocean during 2001, J. Geophys. Res, 110(C7), C07S11, 2005.

González-Dávila, M., Santana-Casiano, J. M., and Ucha, I.: Seasonal variability of fCO_2 in the Angola-Benguela region, Prog. Oceanogr., 83, 124–133, 2009.

González-Dávila, M., Santana-Casiano, J. M., Rueda, M., and Llinás, O.: The water column distribution of carbonate system variables at the ESTOC site from 1995 to 2004, Biogeosciences, 7, 3067-3081, 2010.

Gruber, N. Warming up, turning sour, losing breath: ocean biogeochemistry under global change, Philos. Trans. R. Soc. London, Ser. A, 369 (1943), 1980–1996, 2011.

Gruber, N., Keeling, C. D., and Bates, N. R.: Interannual variability in the North Atlantic Ocean carbon sink, Science, 298(5602), 2374–2378, 2002.

Hagen, E., Schemainda, R. Der Guineadom im ostatlantischen Stromsystem, Beitr. Meereskd., 51, 5–27, 1984.

Hastenrath, S. Climate Dynamics of the Tropics, 488 pp., Kluwer Acad., Norwell, Mass.1995.

Hales, B., Takahashi, T., and Bandstra, L.: Atmospheric CO_2 uptake by a coastal upwelling system, Global Biogeochemical Cycles, 19(1), GB1009, 2005.

Keeling, R. F., Kortzinger, A., and Gruber, N.: Ocean deoxygenation in a warming world, Annu. Rev. Mar. Sci., 2, 199–229; doi:10.1146/annurev.marine.010908.163855, 2010.

Key, R., Kozyr, A., Sabine, C., Lee, K., Wanninkhof, R., Bullister, J., Feely, R., Millero, F. J., Mordy, C., and Peng, T. - H.: A global ocean carbon climatology: Results from GLODAP, Global Biogeochem. Cycles, 18, GB4031, 2004.

Lachkar, Z., and Gruber, N.: Response of biological production and air–sea CO_2 fluxes to upwelling intensificationin the California and Canary Current Systems, J. Mar. Sys., 109–110, 149–160, 2013.

Lee, K., Tong, L. T., Millero, F. J., Sabine, C. L., Dickson, A. G., Goyet, C., Park, G. H., Wanninkhof, R., Feely, R. A., and Key, R. M.: Global relationships of total alkalinity with salinity and temperature in surface waters of the world's oceans, Geophys. Res. Let. 33, L19605, doi:10.1029/2006GL027207, 2006.

Lüger, H., Wallace, D. W., Körtzinger, A., and Nojiri, Y.: The pCO_2 variability in the midlatitude North Atlantic Ocean during a full annual cycle, Global Biogeochem. Cycles, 18(3), GB3023, doi:10.1029/2003GB002200, 2004.

Lüger, H., Wanninkhof, R., Wallace, D. W., and Körtzinger, A.: CO_2 fluxes in the subtropical and subarctic North Atlantic based on measurements from a volunteer observing ship, J. Geophys. Res., 111, C06024, doi:10.1029/2005JC003101, 2006.

Marcello, J., Alonso, H., Eugenio, F, and Fonte, A, Seasonal and temporal study of the northwest African upwelling system, Int. J. Remote Sens., 32:7, 1843-1859, doi:10.1080/01431161003631576, 2011.

Mehrbach, C., Culberson, C. H., Hawley, J. E., Pytkowicz, R. N.: Measurement of the apparent dissociation constants of carbonic acid in seawater at atmospheric pressure, Limnol. Oceanogr., 18, 897–907, 1973.

Michaels, A. F., Karl, D. M., and Capone, D. G.: Element stoichiometry, new production and nitrogen fixation, Oceanography, 14(4), 68–77, 2001.

Mittelstaedt, E.: The upwelling area off Africa—A description of phenomena related to coastal upwelling, Prog. Oceanogr., 12, 307–331, doi:10.1016/0079-6611(83)90012-5., 1983.

Neuer, S., Torres-Padrón, M. E., Gelado-Caballero, M. D., Rueda, M. J., Hernández-Brito, J. J., Davenport, R., and Wefer, G.: Dust deposition pulses to the eastern subtropical

North Atlantic gyre: Does ocean's biogeochemistry respond?, Global Biogeochem. Cycles, 18, GB4020, doi:10.1029/2004GB002228, 2004.

Nicholson, S. E.: Rainfall and atmospheric circulation during drought periods and wetter years in West Africa, Monthly Weather Review, 109(10), 2191–2208, 1981.

Nightingale, P. D., Malin, G., Law, C. S., Watson, A. J., Liss, P. S., Liddicoat, M. L., Boutin, J., and Upstill-Goddard, R. C: In situ evaluation of air-sea gas exchange parameterizations using novel conservative and volatile tracers. Global. Biogeochem. Cycles, 14, 373-387, 2000.

Nykjaer, L., and Van Camp, L.: Seasonal and interannual variability of coastal upwelling along Northwest Africa and Portugal from 1981 to 1991, J. Geophys. Res., 99, 14197–14207, 1994.

Oerder, V., Colas, F., Echevin, V., Codron, F., Tam, J., and Belmadani, A.: Peru-Chile upwelling dynamics under climate change, J. Geophys. Res. Ocean, 120, 1152–1172, doi:10.1002/ 2014JC010299, 2015.

Padín, X., Vázquez-Rodríguez, M., Castaño, M., Velo, A., Alonso-Pérez, F., Gago, J., Gilcoto, M., Álvarez, M., Pardo, P., de La Paz, M., Rios, A. F., and Perez, F. F.: Air-Sea CO_2 fluxes in the Atlantic as measured during boreal spring and autumn, Biogeosciences, 7, 1587–1606, 2010.

Santana-Casiano, J., González-Dávila, M., and Ucha, I.: Carbon dioxide fluxes in the Benguela upwelling system during winter and spring: A comparison between 2005 and 2006, Deep Sea Res. II, 56(8), 533–541, 2009.

Santana-Casiano, J. M., González-Dávila, M., Rueda, M., Llinás, O., and González-Dávila, E- F.: The interannual variability of oceanic CO_2 parameters in the northeast Atlantic subtropical gyre at the ESTOC site, Global Biogeochem. Cycles, 21(1), GB1015, doi:10.1029/2006GB002788, 2007.

Santos, A. M. P., Kazmin, A. S., and Peliz, A.: Decadal changes in the Canary upwelling system as revealed by satellite observations: Their impact on productivity, J. Mar. Res., 63, 359–379, 2005.

Santos, F., de Castro, M., Gómez-Gesteira, M., and Alvarez, I.: Differences in coastal and oceanic SST warming rates along the Canary upwelling ecosystem from 1982 to 2010, Continental Shelf Res., 47, 1-6, 2012.

Schuster, U., Watson, A., Bates, N., Corbiere, A., Gonzalez-Davila, M., Metzl, N., Pierrot. D., and Santana-Casiano, J. M.: Trends in North Atlantic sea-surface fCO_2 from 1990 to 2006, Deep Sea Res. II, 56(8), 620–629, 2009.

Takahashi, T., Olafsson, J., Goddard, J. G., Chipman, D. W., and Sutherland, S.: Seasonal variation of CO_2 and nutrients in the high-latitude surface oceans: A comparative study, Glob. Biogeochem. Cycles, 7(4), 843–878, 1993.

Takahashi, T., Sutherland, S., Wanninkhof, R., Sweeney, C., Feely, R., Chipman, D., Hales, B., Friederich, G., Chavez, F., Sabine, C., Watson, A., Bakker, D., Schuster, U., Metzl, N., Yoshikawa-Inoue, H., Ishii, M., Midorikawa, T., Nojiri, Y., Kortzinger, A., Steinhoff, T., Hoppema, M., Olafsson, J., Arnarson, T., Tilbrook, B., Johannessen, T., Olsen, A., Bellerby, A., Wong, C., Delille, B., Bates, N., and de Baar, H.: Climatological mean and decadal change in surface ocean pCO_2, and net sea-air CO_2 flux over the global oceans, Deep-Sea Res. II, 56(8-10), 554–577, 2009.

Ullman, D. J., McKinley, G. A., Bennington, V., and Dutkiewicz, S.: Trends in the North Atlantic carbon sink: 1992–2006, Glob. Biogeochem. Cycles, 23(4), doi:10.1029/2008GB003383, 2009.

Varela, R., Álvarez, I., Santos, F., de Castro, M., Gómez-Gesteira, M.: Has upwelling strengthened along worldwide over 1982-2010?, Sci. Rep. **5**, 10016; doi:10.1038/srep10016, 2015.

Wang, Y., Castelao, R. M., and Yuan, Y.: Seasonal variability of alongshore winds and sea surface temperature fronts in Eastern Boundary Current Systems, J. Geophys. Res. Oceans, 120, 2385–2400; doi:10.1002/2014JC010379, 2015.

Watson, A., Schuster, U., Bakker, D., Bates, N., Corbière, A., González-Dávila, M., Friedrich, T., Hauck, J., Heinze, C., Johannessen, T., Kortzinger, A., Metzl, N., Olafsson, J., Olsen, A., Oschlies, A., Padin, X. A., Pfeil, B., Santana-Casiano, J. M., Steinhoff, T., Telszewski, M., Rios, A. F., Wallace, D. W., and Wanninkhof, R.: Tracking the variable North Atlantic sink for atmospheric CO_2, Science, 326(5958), 1391–1393, doi:10.1126/science.1177394, 2009.

Yoo, J.-M. and Carton, J. A.: Annual and interannual variation of the freshwater budget in the tropical Atlantic Ocean and the Caribbean Sea, J. Phys. Oceanogr., 20(6), 831–845, 1990.

LEGEND FOR FIGURES

Fig. 1. Ship track in the area from 28ºN (Gran Canaria, The Canary Islands) to 10ºN (black dots). The locations of Cap Blanc and Cape Verde are indicated. Monthly Ocean Color (oceancolor.gsfc.nasa.gov) data for average chlorophyl *a* concentration (mg m^{-3}) were included in a MatlabTM routine and annually averaged. The map has been generated using Matlab 7.12 R2011a.

Fig. 2. Time series of upwelling index (UI*10^{-3} m^2 s^{-1}) in the Mauritanian-Cape Verde upwelling region along the ship track computed following Nykjaer and Van Camp (1994). Cool colours are related to upwelling events and warm colours to downwelling events.

Fig. 3. *In situ* data of a) SST and b) SSS data in the Mauritanian - Cape Verde coastal region grouped by seasons: winter (W, December, January and February), spring (Sp, March, April and May), summer (Sm, June, July and August) and autumn (Au, September, October and November). The averaged values for all cruises in Table S1, are shown in black for each season including the 95% confidence limits. Colour code for each cruise is that indicated in Table S1.

Fig. 4. Latitudinal distribution of the interannual trends for the Upwelling Index (UI*10^{-3}) and for the four experimental variables along the QUIMA-VOS line integrated over every degree between 2005 and 2012. The a) panel presents the trends for Upwelling index (UI*10^{-3} m^2 s^{-1}, mean confidence interval of 9 m^2 s^{-1}), SST (ºC yr^{-1}, confidence interval 0.13ºC) and SSS (yr^{-1}, confidence interval 0.06) and the b) panel the trends for fCO_2^{sw} and fCO_2^{atm} (confidence intervals 4.23 µatm and 0.44 µatm).

Fig 5. Fugacity of CO_2 data in the Mauritanian-Cape Verde coastal region grouped by seasons: winter (W, December, January and February), spring (Sp, March, April and May), summer (Sm, June, July and August) and autumn (Au, September, October and

November). a) fCO_2^{sw} latitudinal distribution. b) Difference between measured and Normalized fCO_2^{sw} values to a constant temperature of 22ºC. The averaged values for all cruises in Table S1, are shown in black for each season including the 95% confidence limits. Colour code for each cruise is that indicated in Table S1.

Fig. 6. pH at *in situ* SST in total proton scale computed from total alkalinity (based on regional correlations with SST and SSS, Lee et al., 2006) and fCO_2 at 21 ± 0.25 ºN. The error bar represents the standard deviation of the computed data for each cruise for the selected latitude. The black line shows the harmonic fitting Eq. (4) for the data and the corresponding linear trend.

Fig. 7. Latitudinal distribution of seasonal and annual CO_2 fluxes, FCO_2 (mol m^{-2}). Fluxes of CO_2 were computed using Nightingale et al. (2000) parametrization and satellite winds with a resolution of 6 hours. a) Integrated year-to-year from 2005 to 2012 and b) latitudinally integrated for 2005 to 2012 together with annual values for NAO index. Latitudinal distribution of FCO_2 seasonally integrated from 2005 to 2012 are depicted for winter (c, December, January and February), spring (d, March, April and May), summer (e, June, July and August) and autumn (f, September, October and November).

767 Fig. 1

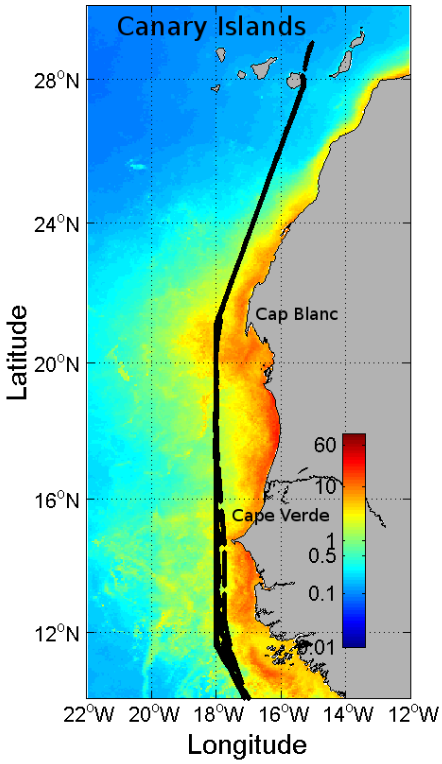

Canary Islands
28°N
24°N
Cap Blanc
20°N
Latitude
60
10
16°N
Cape Verde
1
0.5
0.1
12°N
0.01
22°W 20°W 18°W 16°W 14°W 12°W
Longitude

768

Fig. 2

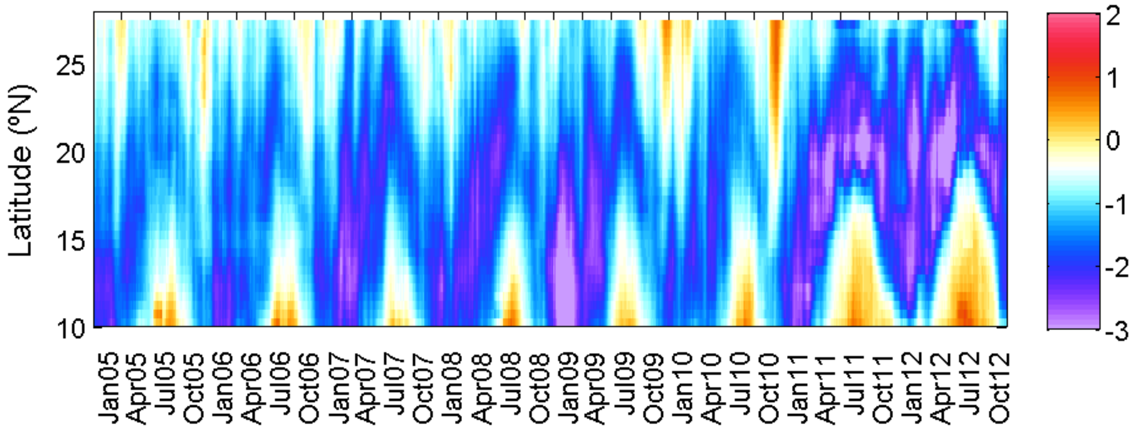
Latitude (ºN)
25
20
15
10
Jan05
Apr05
Jul05
Oct05
Jan06
Apr06
Jul06
Oct06
Jan07
Apr07
Jul07
Oct07
Jan08
Apr08
Jul08
Oct08
Jan09
Apr09
Jul09
Oct09
Jan10
Apr10
Jul10
Oct10
Jan11
Apr11
Jul11
Oct11
Jan12
Apr12
Jul12
Oct12
2
1
0
-1
-2
-3

Fig. 3

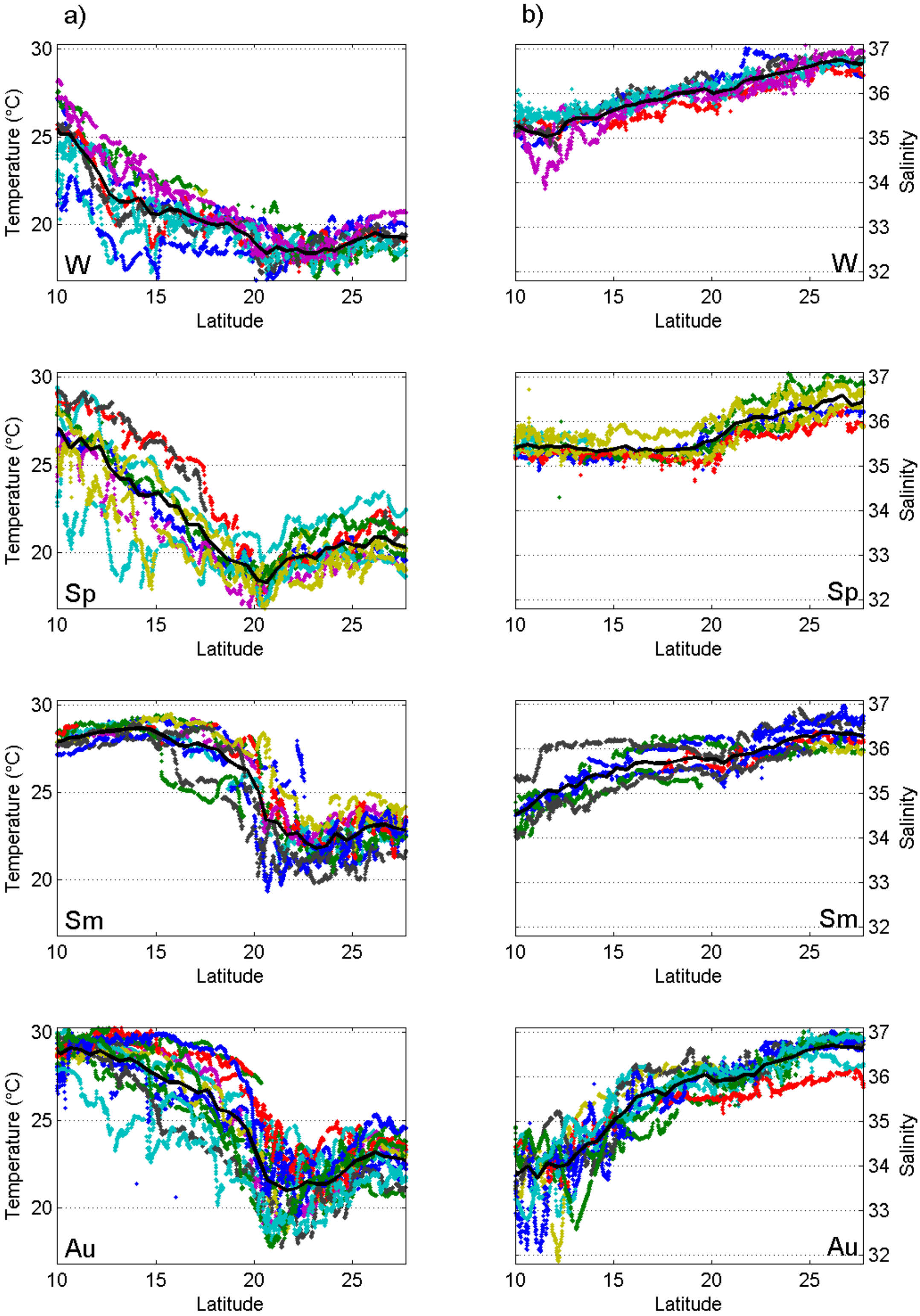

Fig. 4

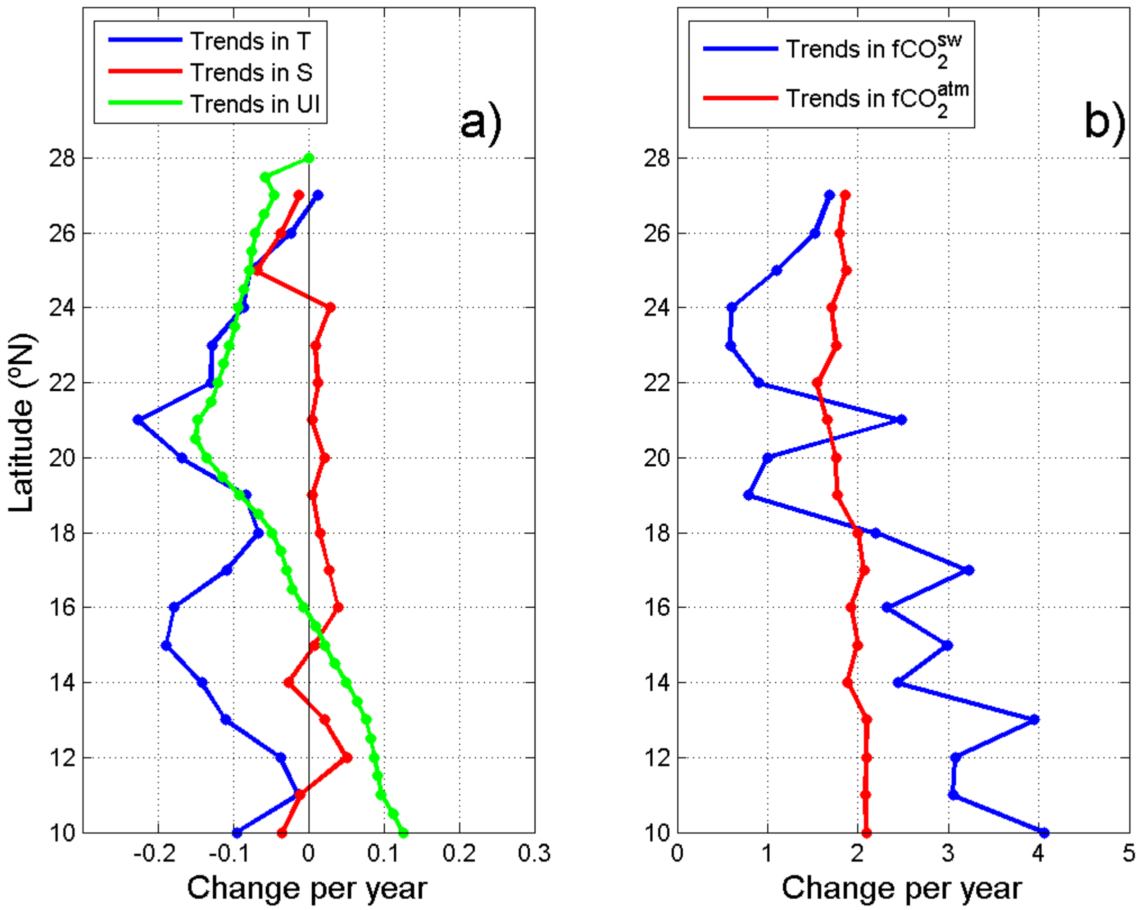

Trends in T
Trends in S
Trends in UI
a)
Latitude (ºN)
28
26
24
22
20
18
16
14
12
10
-0.2
-0.1
0
0.1
0.2
0.3
Change per year
Trends in fCO_2^{sw}
Trends in fCO_2^{atm}
b)
28
26
24
22
20
18
16
14
12
10
0
1
2
3
4
5
Change per year

Fig. 5

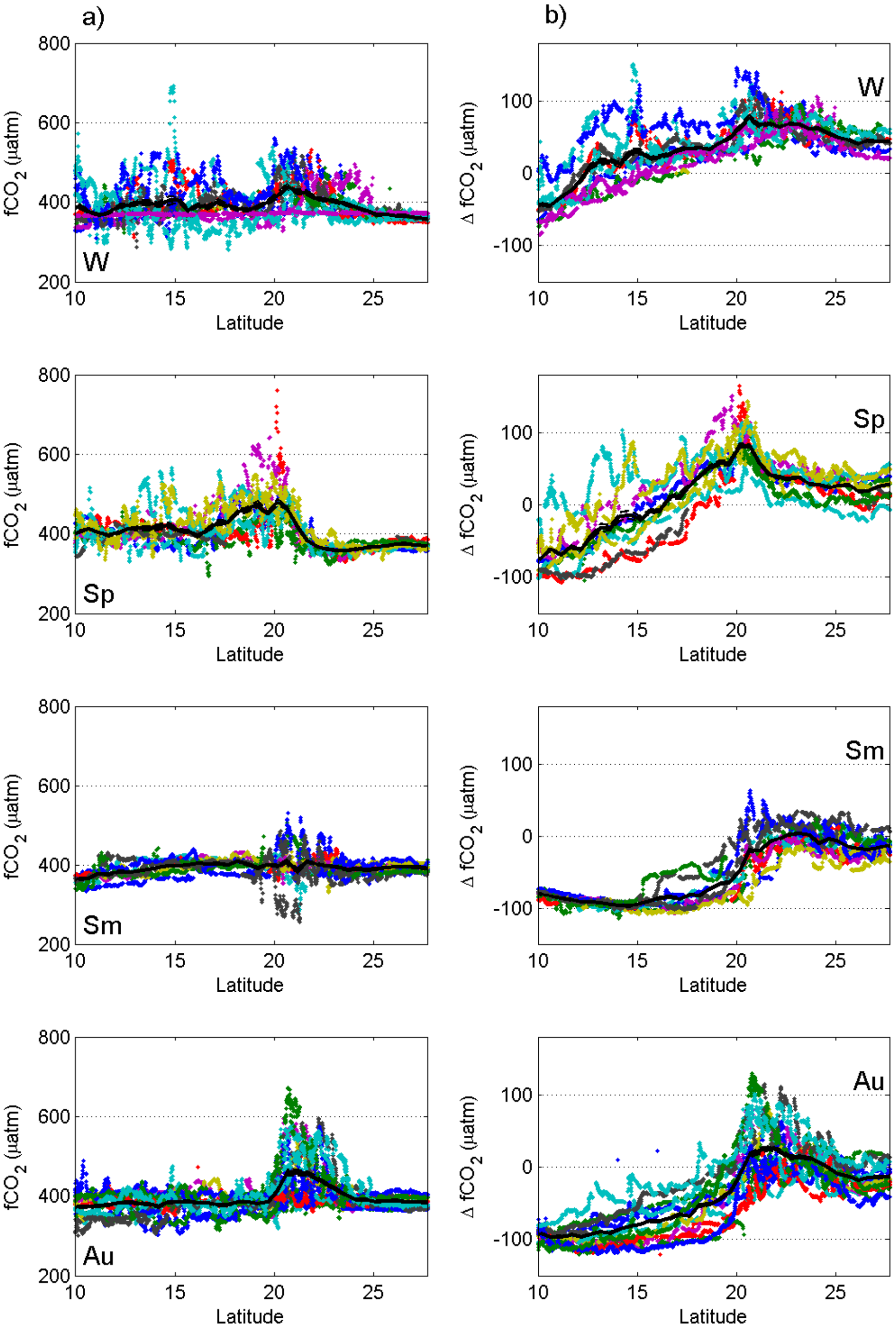
a)
b)
fCO2 (µatm)
Δ fCO2 (µatm)
Latitude
W
Sp
Sm
Au
800
600
400
200
100
0
-100
10
15
20
25

Fig. 6

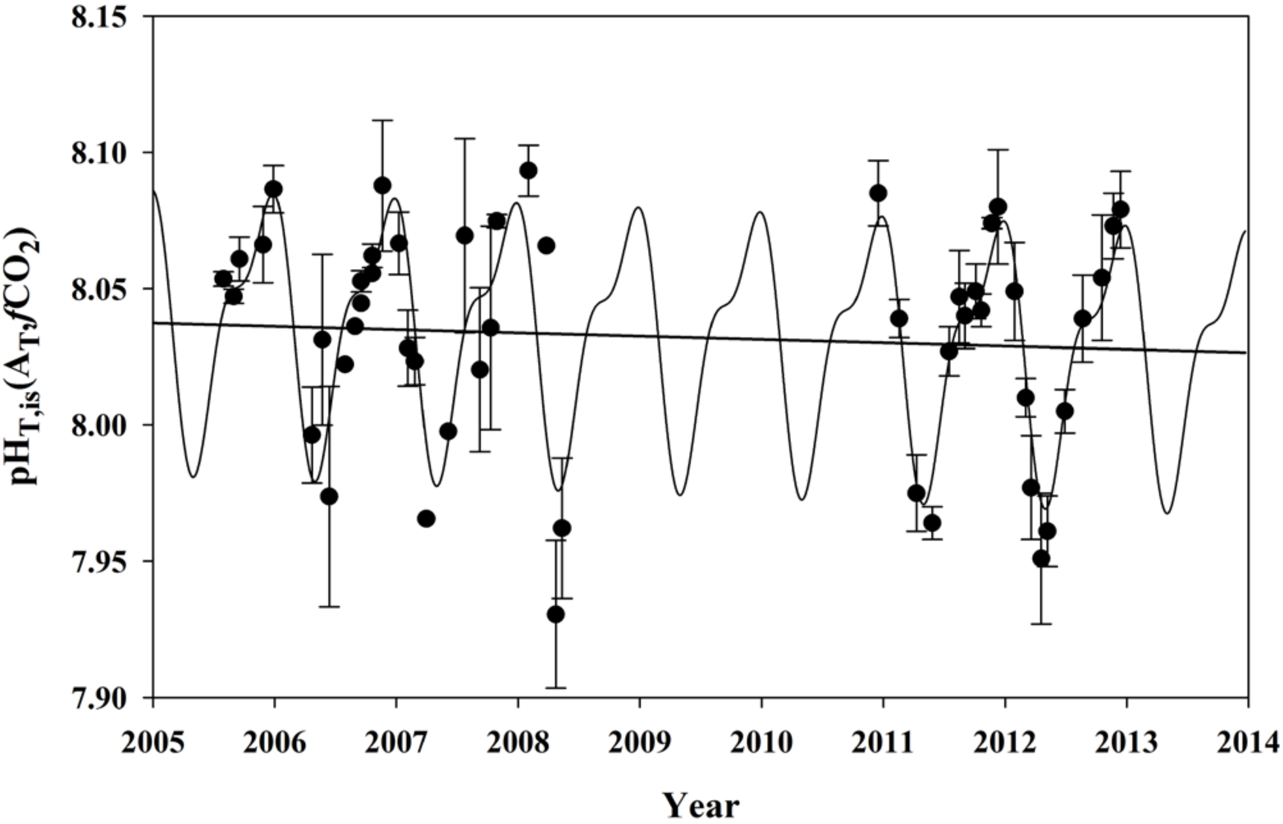
8.15
8.10
8.05
8.00
7.95
7.90
$pH_{T,is}(A_T, fCO_2)$
2005
2006
2007
2008
2009
2010
2011
2012
2013
2014
Year

Fig. 7

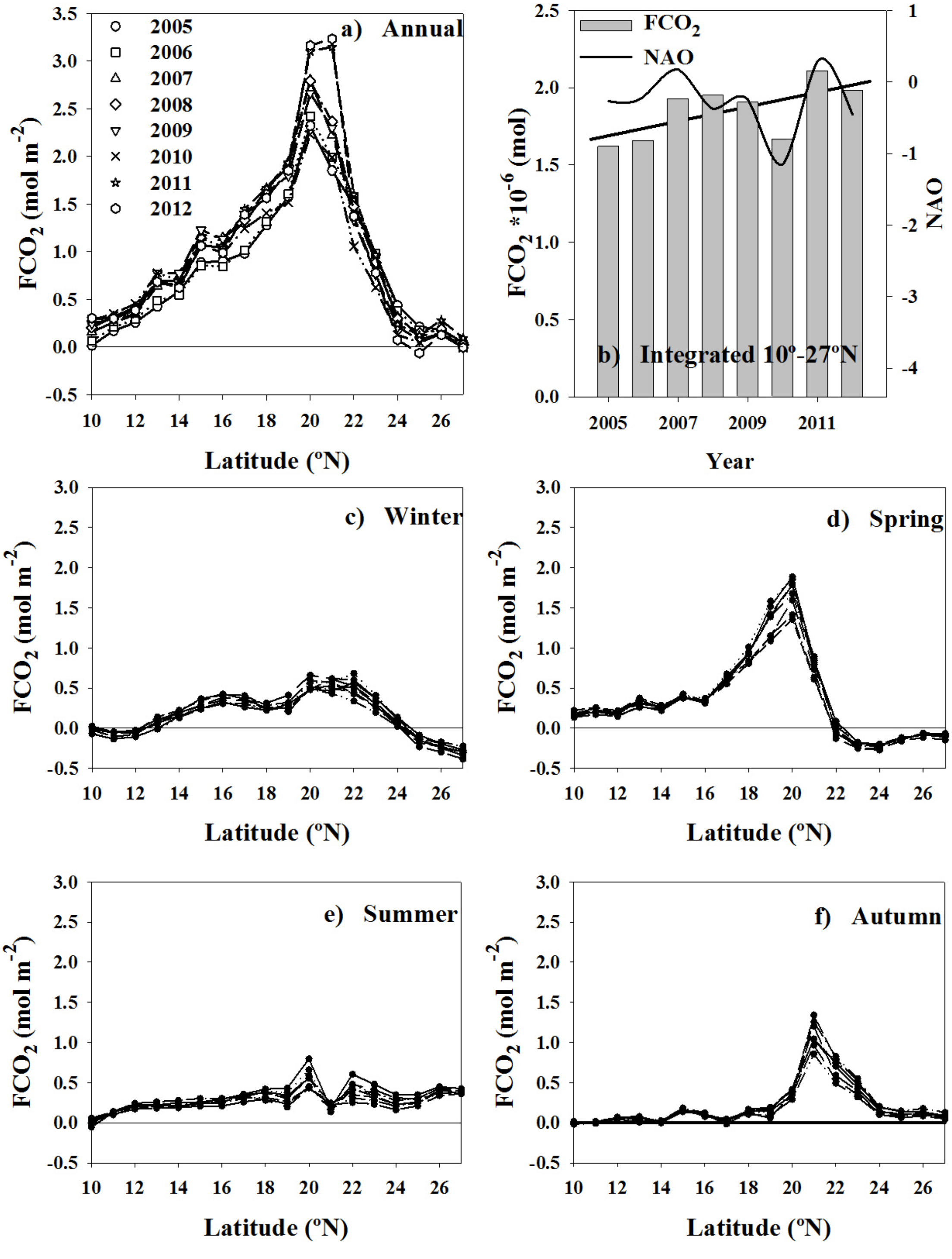
a) Annual
2005
2006
2007
2008
2009
2010
2011
2012
FCO$_2$ (mol m^{-2})
Latitude (ºN)
b) Integrated 10º-27ºN
FCO$_2$
NAO
FCO$_2$ *10^{-6} (mol)
Year
2005
2007
2009
2011
c) Winter
d) Spring
e) Summer
f) Autumn